Supporting Information for *Acta Phys. -Chim. Sin.* doi: 10.3866/PKU.WHXB202106002

镶嵌于NH_2-MIL-125 (Ti)衍生氮掺多孔碳中的花状超细纳米TiO_2作为高活性和稳定性的锂离子电池负极材料

杨越 [1,2]，朱加伟 [1]，王鹏彦 [1]，刘海咪 [1]，曾炜豪 [1]，陈磊 [1]，陈志祥 [1]，木士春 [1,2,*]

[1] 武汉理工大学，材料复合新技术国家重点实验室，武汉 430070

[2] 佛山仙湖实验室，先进能源科学与技术广东省实验室佛山分中心，广东 佛山 528200

NH_2-MIL-125 (Ti) Derived Flower-Like Fine TiO_2 Nanoparticles Implanted in N-doped Porous Carbon as an Anode with High Activity and Long Cycle Life for Lithium-Ion Batteries

Yue Yang [1,2], Jiawei Zhu [1], Pengyan Wang [1], Haimi Liu [1], Weihao Zeng [1], Lei Chen [1], Zhixiang Chen [1], Shichun Mu [1,2,*]

[1] State Key Laboratory of Advanced Technology for Materials Synthesis and Processing, Wuhan University of Technology, Wuhan 430070, China.

[2] Foshan Xianhu Laboratory of the Advanced Energy Science and Technology Guangdong Laboratory, Xianhu hydrogen Valley, Foshan 528200, Guangdong Province, China.

[*]Corresponding author. Email: msc@whut.edu.cn.

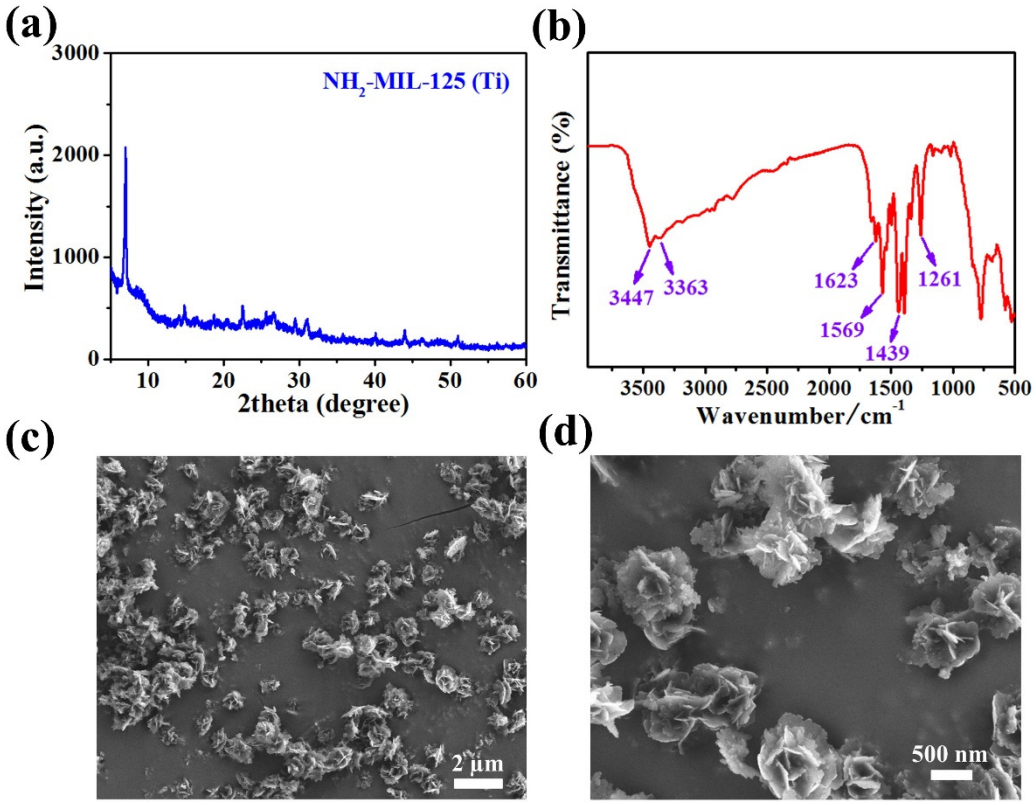

Fig. S1 XRD patterns (a) of NH_2-MIL-125 (Ti). FTIR spectrum (b) of NH_2-MIL-125 (Ti). SEM images of NH_2-MIL-125 (Ti) (c, d).

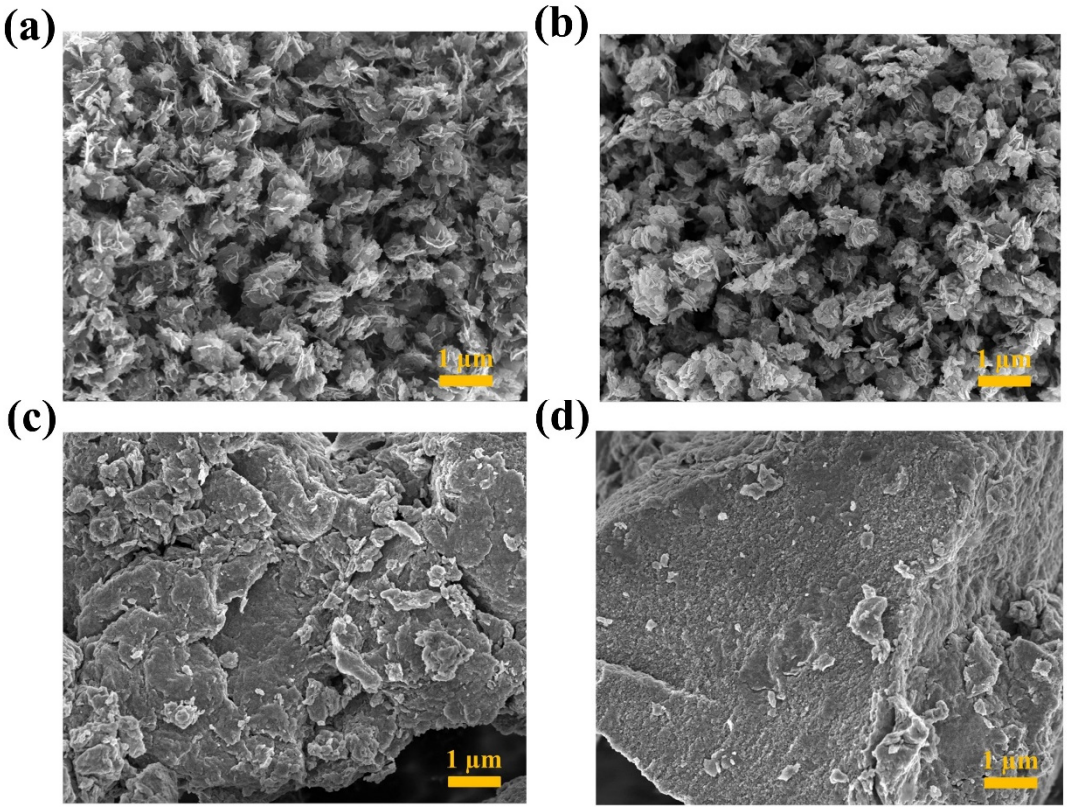

Fig. S2 Low magnification SEM images of FL-TiO_2/NPC (a, b) and P-TiO_2 (c, d).

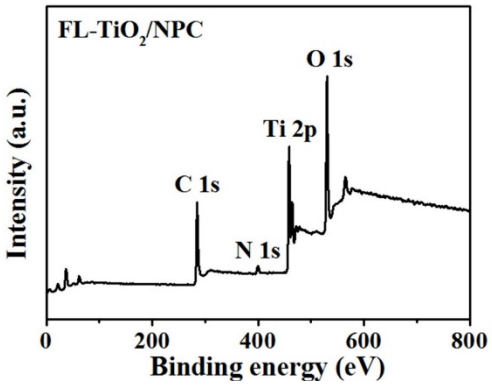

Fig. S3 Full XPS spectrum of FL-TiO_2/NPC.

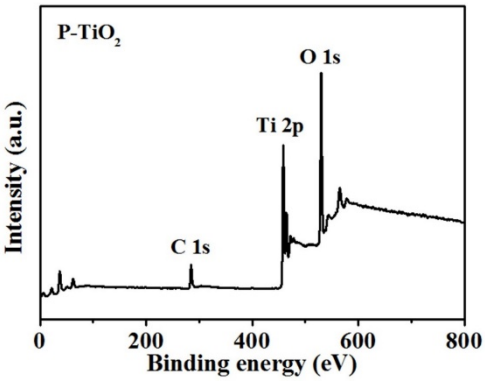

Fig. S4 Full XPS spectrum of P-TiO_2.

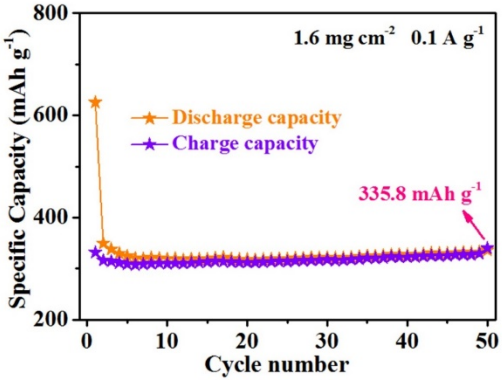

Fig. S5 Long-term cycling performance with high loading of FL-TiO_2/NPC at 0.1 A·g^{-1}.

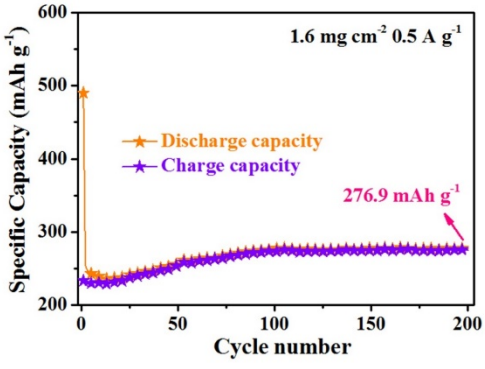

Fig. S6 Long-term cycling performance with high loading of FL-TiO_2/NPC at 0.5 A·g^{-1}.

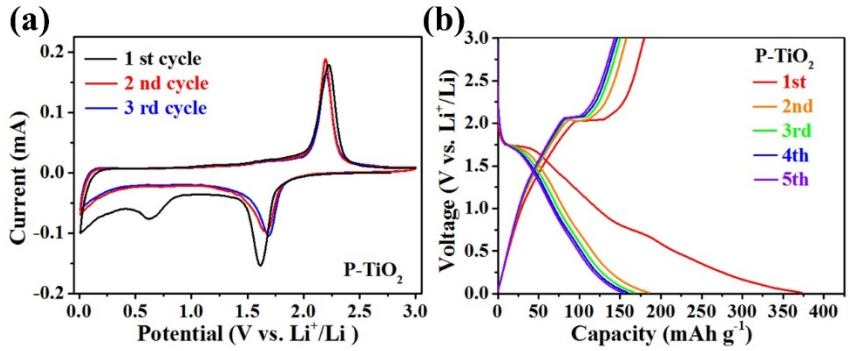

Fig. S7 CV plots (a) of P-TiO₂ for the first three cycles at a scan rate of 0.1 mV·S^{-1} in the voltage range of 0.01–3 V. Discharge/charge curves of voltage range at a current density of 0.2 A·g^{-1} for the first five cycles (b) of P-TiO₂.

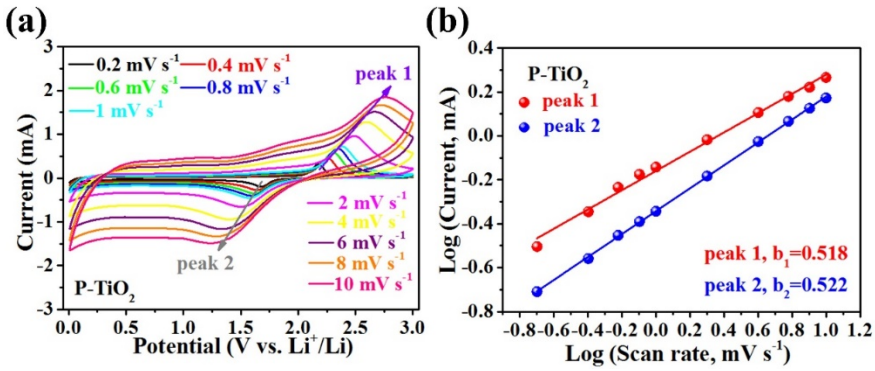

Fig. S8 CV curves of P-TiO₂ at different scan rate of 0.2–10.0 mV·s^{-1} (a). Calculation of the b values by plotting log*i* versus log*v* (b).

Table S1 Comparison of the electrochemical Li-storage performance of TiO₂/carbon composites in other literature.

Composites	Discharge capacity (mAh·g^{-1})/cycle (test window)	Current density (mA·g^{-1})	Loading mass	Ref.
FL-TiO₂/NPC	256.5/2000 (0.01–3.0 V)	2000	~0.8 mg·cm^{-2}	This work
TiO₂/Foam-like 3D mesoporous N-doped carbon	Average 227/200 (0.01–3.0 V)	335	0.5–0.8	*J. Power Sources* **2019,** *420*, 38.
TiO₂@N-doped carbon coaxial nanotubes	235/500 (0.01–3.0 V)	500	–	*Appl. Surf. Sci.* **2018,** *458*, 1018.
TiO₂/C nanofibers	176/2000 (0.01–3.0 V)	3350	1.8–2.3 mg·cm^{-2}	*ACS Appl. Mater. Interfaces* **2018,** *10*, 35060.
Mesoporous TiO₂/carbon microsphere	235.8/200 (1.2–2.8 V)	335	–	*Ceram. Int.* **2018,** *44*, 14, 16265.
Hollow urchin-like TiO₂/N-doped carbon	165.1/200 (1.0–3.0 V)	837.5	–	*J. Power Sources* **2018,** *385*, 10.
NCF@CNTs-TiO₂	90.58/2500 (1.0–3.0 V)	1680	~1.5 mg·cm^{-2}	*J. Power Sources* **2018,** *379*, 10.
N-doped carbon/TiO₂ coaxial nanofibers	149/500 (0.01–3.0 V)	1000	–	*J. Am. Ceram. Soc.* **2017,** *100*, 2939.
Mesoporous TiO₂@N-doped C nanospheres	117/2000 (1.0–3.0 V)	1680	–	*Nanoscale* **2017,** *9*, 1539.
TiO₂-B nanosheets with N-doped carbon	210/2230 (1.0–3.0 V)	500	~1.5–2 mg·cm^{-2}	*J. Mater. Chem. A* **2016,** *4*, 8172.
Mesoporous TiO₂ microfibers@ N-doped carbon	119.1/500 (1.0–3.0 V)	1700	1.58 mg·cm^{-2}	*Nanoscale* **2015,** *7*, 13898.
N-doped TiO₂ nanorods/carbon dots	185/1000 (1.0–3.0 V)	1680	1.1 mg·cm^{-2}	*J. Mater. Chem. A* **2015,** *3*, 5648.
Anatase TiO₂/N-doped carbon	180.9/500 (0.02–3.0 V)	500	3.0 mg	*J. Power Sources* **2015,** *273*, 472.

Battery assembly and electrochemical measurements: The electrochemical performances of the FL-TiO_2/NPC and P-TiO_2 composites were investigated by assembling the CR2016 coin-type Li-metal cells. Working electrodes were comprised of 80% active materials (the FL-TiO_2/NPC and P-TiO_2), 10% super conductive carbon, and 10% poly (vinylidene fluoride) (PVDF). These materials were dispersed in an appropriate amount of N-methy-2-pyrrolidone (NMP) and ground thoroughly for half an hour. The homogenous slurry was pasted uniformly onto the Cu foil, followed by vacuum drying at 80 °C for 24 h. The Cu foil was cut into small round pieces with an area of 0.785 cm^2. After weighing and calculation, the active material mass loading was about 0.8 $mg \cdot cm^{-2}$. 1M $LiPF_6$ dissolved in dimethyl carbonate (DMC) and ethylene carbonate (EC) (volume ratio 1 : 1) was used as electrolyte. The all half cells were assembled in an Ar-filled glovebox with the content of oxygen and moisture below 0.5 ppm. Li foil was used as the counter electrode and Celgard 2500 film was chosen as the separator. The galvanostatic cycling test of all cells was carried out on a Neware CT-3008W battery test system between 0.01 and 3 V at room temperature. The cyclic voltammetry (CV) measurements was performed on CHI 760E (Shanghai Chenhua Instruments Corp., Ltd.) electrochemical workstation in a voltage of 0.01–3.0 V *vs*. Li/Li^+ with a scan rate of 0.1 $mV \cdot s^{-1}$. The electrochemical impedance spectroscopy (EIS) with the frequency range from 0.01 to 100 kHz was performed on a CS 350H (Wuhan Corrtest Instruments Corp., Ltd.) electrochemical workstation.

Materials characterization: The crystal structure of as-prepared the FL-TiO_2/NPC and P-TiO_2 were performed on a Bruker D8 Advance with a Cu K_α radiation source. The morphology was studied by JEM-7500F field emission scanning electron microscopy (FESEM Zeiss Ultra Plus). The microstructure was performed by using the high-resolution transmission electron microscope (HRTEM, Talos F200S) fitted with energy-dispersive X-ray spectroscopy analyzer. The elemental composition and thermal-stability were characterized by using X-ray photoelectron spectroscopy (XPS) analyses with Mg as an excitation source (VG MultiLab 2000 spectrometer), the Raman analysis (Renishaw UV-1000), the thermogravimetric analysis (TGA, Netzsch TG209F3). The specific surface area and pore distribution were calculated by using the Brunauer-Emmett-Teller analysis (BET, Micromeritics Tristar II3020, 77 K).